Capacity and Nonuniform Signaling for Discrete-Time Poisson Channels

Jihai Cao, Steve Hranilovic, and Jun Chen

***Abstract*—The Poisson photon-counting model is accurate for optical channels with low received intensity, such as long-range intersatellite optical wireless links. This work considers the computation of the channel capacity and the design of capacity-approaching, nonuniform signaling for discrete-time Poisson channels in the presence of dark current and underaverage and peak amplitude constraints. Although the capacity of this channel is unknown, numerical computation of the channel capacity is implemented using a particle method. A nonuniform mapper is coupled to a low-density parity check code and a joint demapper–decoder is designed based on the sum-product algorithm. Simulations indicate near-capacity performance of the proposed coding system and significant gains over information rates using traditional uniform signaling. A key observation of this work is that significant gains in rate can be achieved for the same average power consumption by using optical transceivers with nonuniform signaling and a modest increase in peak power.**

***Index Terms*—Channel capacity; Discrete-time Poisson channel; Intersatellite optical communications; Nonuniform signaling.**

I. Introduction

A practical model for low-power optical communication channels is the discrete-time Poisson channel [1–3]. These channels exist in long-range optical communications such as intersatellite laser links. For satellite applications, free-space optical (FSO) communications provides larger bandwidth, smaller beam divergence, and higher antenna gains from smaller apertures as compared with rf transceivers. This high gain translates into a significant reduction in the required transceiver power, volume, and mass. Recently, an optical link between two low-Earth-orbit (LEO) satellites has been demonstrated at a rate of 5.625 Gbps over a range of 3800–4900 km with a telescope diameter of 12.5 cm, a total mass of 32 kg, and a power consumption of less than 120 W for the entire transceiver [4].

In discrete-time Poisson channels, the intensity of the transmitter is pulse amplitude modulated (PAM) in discrete time slots. Both the mean, ε, and peak, A, emitted intensities (i.e., power) are constrained due to energy and component limitations on spacecraft. In addition, all received counts are corrupted by dark current. Currently, no closed-form expression exists for the capacity of this channel. In [5], Shamai showed that the capacity-achieving distribution for the discrete-time Poisson channel with peak amplitude constraint is *discrete* and has a *finite* number of probability mass points. Lapidoth and Moser [6] derived asymptotic bounds on the capacity of the discrete-time Poisson channel with dark current as ε and A tend to infinity, but their ratio is fixed. The bounds are asymptotically tight but often are quite loose at low ε. In [7] capacity bounds on the discrete-time Poisson channel are given asymptotically as $\varepsilon \to 0$ with A fixed. The bounds, however, are loose for all but very small input powers. In [8], Martinez obtained tight upper and lower capacity bounds with no dark current and with only an average amplitude constraint.

Signaling design for discrete-time Poisson channels often involves complex optimization to find the discrete capacity-achieving distribution. Once a distribution is found, a deterministic mapper is designed to induce the correct nonuniform distribution [9]. Multilevel coding (MLC) and multistage decoding (MSD) have been used with a mapper to approach the capacity of terrestrial FSO channels with Gaussian noise [10,11].

In this work, the capacity of the discrete-time Poisson channel is computed by extending a particle-based algorithm [12] to find both the capacity and required input distribution. Unlike earlier work, this approach produces a sequence of upper and lower bounds that converge in practice and are computationally efficient even for large ε and A. In addition, a constrained particle algorithm is presented that produces constellations with quantized probability masses. The resulting constellations have rates close to the channel capacity and often require fewer mass points, whereas their simple structure enables straightforward mapper design. In contrast to previous MLC-MSD work, here the nonuniform mapper is combined with a low-density parity check (LDPC) code and a joint demapper–decoder is developed based on the sum-product algorithm. Simulation results in a practical LEO context show large gains in rate, outperforming uniform signaling, at the same average power consumption at a small increase in peak amplitude.

The channel model is rigorously specified in Section II. Section III briefly reviews the numerical techniques used to compute channel capacity, develops tight capacity bounds, and applies these bounds to a realistic LEO intersatellite link. Section IV presents practical algorithms to

Manuscript received April 30, 2012; revised December 13, 2012; accepted January 2, 2013; published January 3, 2013 (Doc. ID 167583).

The authors are with the Department of Electrical and Computer Engineering, McMaster University, Hamilton, Ontario, Canada (e-mail: hranilovic@ece.mcmaster.ca; e-mail: junchen@ece.mcmaster.ca).

Digitial Object Identifier 10.1364/JOCN.5.099999

approach the channel capacity and demonstrates their operation in a variety of scenarios, including the LEO intersatellite link. The paper concludes in Section V with suggestions for future work.

II. Channel Model

In discrete-time Poisson channels, data are transmitted by sending PAM intensity signals that are constant in discrete time slots. In contrast to continuous-time Poisson channels, which admit arbitrary waveforms, the discrete-time Poisson model imposes a bandwidth limit by constraining transmitted signals to be rectangular PAM. The PAM amplitudes are limited to $\mathbb{R}^+$ since the underlying quantity modulated is the optical intensity.

In addition, due to device constraints and limited energy storage on the spacecraft, both the mean, ε, and peak intensity, A, must be constrained. The receiver is a photon counter that outputs an integer representing the number of received photons. Specifically, in each time slot, given channel input x, the channel output y obeys the Poisson distribution with average value $x+\lambda$, that is,

$$P_{Y|X}(y|x) = \frac{(x+\lambda)^y}{y!}e^{-(x+\lambda)}, \qquad x \in \mathbb{R}^+, \qquad y \in \mathbb{Z}^+, \quad (1)$$

where λ represents the combined impact of background radiation and average dark current. Although intersatellite links operate above the atmosphere, unintended light scattered from the Earth as well as from other planets and stars will impinge on the receiver [13]. Dark current represents the detector nonideality and corrupts the received counts even in the absence of illumination [14, Ch. 5]. Dark current arises in all photodetectors and is a fundamental limitation on the performance of any optical receiver. Furthermore, the constraints of the input signal x are

$$0 \le X \le A \quad \text{and} \quad \mathbb{E}(X) \le \varepsilon.$$

The channel capacity, C, of a discrete-time Poisson channel is the maximum mutual information over input distributions satisfying channel constraints, namely,

$$C \triangleq \max_{p_X(\cdot)\epsilon\mathcal{P}} I(X;Y) = \max_{p_X(\cdot)\epsilon\mathcal{P}} \int_x p_X(x) \times \left[\sum_y P_{Y|X}(y/x)\log\frac{P_{Y|X}(y|x)}{P_Y(y)}\right]\mathrm{d}x, \quad (2)$$

where

$$\mathcal{P} \triangleq \left\{p_X(x)\colon \int_0^A p_X(x)\mathrm{d}x = 1, p_X(x) \ge 0, \mathbb{E}_{p_X(\cdot)}\{X\} \le \varepsilon\right\}.$$

III. Channel Capacity And Nonuniform Signaling

A. Capacity Computation

The Blahut–Arimoto algorithm [15] can be used to find the channel capacity and input distribution for constrained channels where input and output are chosen from discrete finite sets. In [12], the algorithm is extended to channels with continuous input distributions by discretizing them into a list of points termed *particles*. In this section, the techniques in [12,15] are adapted to the discrete-time Poisson channel with peak and average amplitude constraints to compute tight bounds on the capacity and to find the capacity-achieving input distribution. An advantage of this approach is that it is able to produce accurate estimates of the channel capacity even for large values of ε and A. Previous approaches using brute-force optimization techniques suffer from very large dimensionality for large ε and A and take excessive amounts of computing time.

Consider approximating the input probability density for X using a list of particles $\{(x_i, p_i)\}$ to give

$$p_X(x) \approx \hat{p}_X(x) = \sum_{i=1}^{M} p_i\delta(x - x_i),$$

where p_i, $i = 1,\ldots,M$, are real and nonnegative with $\sum_{i=1}^{M} p_i = 1$ and $x_i \in \mathcal{X} = [0,A]$. The value of M must be chosen large enough to ensure the convergence of the algorithm as discussed in [12].

The optimization problem in Eq. (2) is solved iteratively, where $\{(x_i^{(k)}, p_i^{(k)})\}$ denotes the list of particles at the kth step. The list of particles is alternately updated using the following two steps:

$$p^{(k)} \triangleq \arg\max_p I(\{(x^{(k-1)}, p)\}), \qquad (W\text{-step}), \qquad (3)$$

$$x^{(k)} \triangleq \arg\max_x I(\{(x, p^{(k)})\}). \qquad (X\text{-step}). \qquad (4)$$

The W-step in Eq. (3) optimizes the weights p with the positions $x^{(k-1)}$ fixed and can be accomplished by the constrained Blahut–Arimoto algorithm [15] with average constraint ε. The X-step in Eq. (4) maximizes $I(\{(x_i, p_i)\})$ by optimizing the positions with the weights fixed. Practically the X-step is accomplished by means of a steepest ascent technique [12].

After n iterations, a lower bound on the capacity C can be shown to be

$$C \ge L^{(n)} = I(\{(x_i^{(n)}, p_i^{(n)})\}), \quad (5)$$

while an upper bound on C is given by

$$C \le U^{(n)} = \max_{x\in\mathcal{X}}[D(P_{Y|X}(y|x)\|\hat{P}(y)^{(n)}) - s^{(n)}x] + s^{(n)}\sum_{i=1}^{M} p_i^{(n)}x_i^{(n)}, \quad (6)$$

where $s^{(n)}$ is a parameter set to ensure convergence [15].

B. Numerical Results and Analytical Bounds

Figure 1 shows $L^{(n)}$ and $U^{(n)}$ for the discrete-time Poisson channel with $A/\varepsilon = 4$ and $\lambda = 3$ as a function of the average input power. The value of M should be large enough to ensure the convergence of the algorithm, and

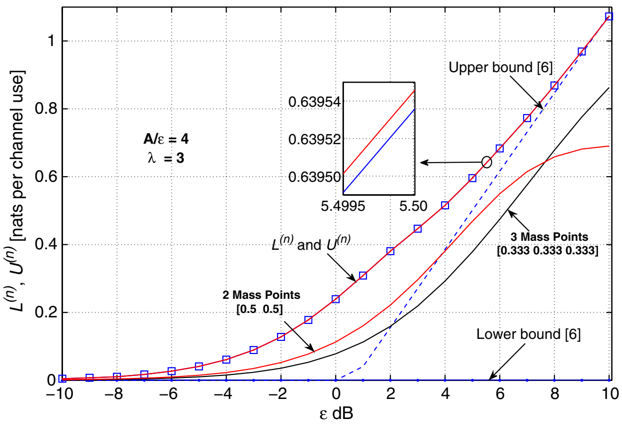

Fig. 1. (Color online) Bounds $L^{(n)}$, $U^{(n)}$ on channel capacity (on top of each other) and closed form bounds from [6] with $A/\varepsilon = 4$ and $\lambda = 3$.

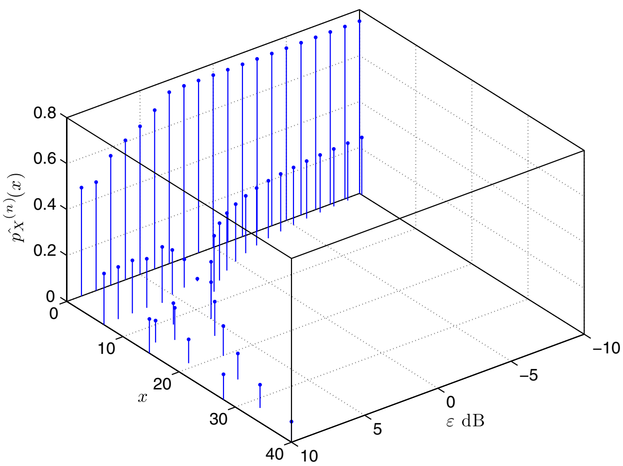

Fig. 2. (Color online) Capacity achieving input distributions for $A/\varepsilon = 4$ and $\lambda = 3$.

in these simulations $M = 200$. It can be seen that both bounds nearly coincide over a wide range of powers. The gap between $L^{(n)}$ and $U^{(n)}$ is about 10^{-5} nats per channel use after 100 iterations, and the accuracy could in fact be improved further by increasing the number of iterations. The lower and upper bounds of Lapidoth and Moser [6, Eqs. (12) and (13)] are also presented for comparison. Notice that due to their asymptotic nature, these bounds yield no insight at lower power levels.

Figure 2 shows the capacity-achieving distributions over ε with $A/\varepsilon = 4$ and $\lambda = 3$. As noted in [5], the capacity-achieving distribution for the discrete-time Poisson channel with average power and peak power constraint is discrete. Notice also that there are always probability mass points at $x_i = 0$. Additionally notice that when $\varepsilon < 3$ dB, the capacity-achieving distributions are nonuniform binary distribution. In Fig. 1, the mutual information for uniform two- and three-point constellations are also plotted. There is a large gap in the mutual information using equiprobable constellations and the channel capacity, which

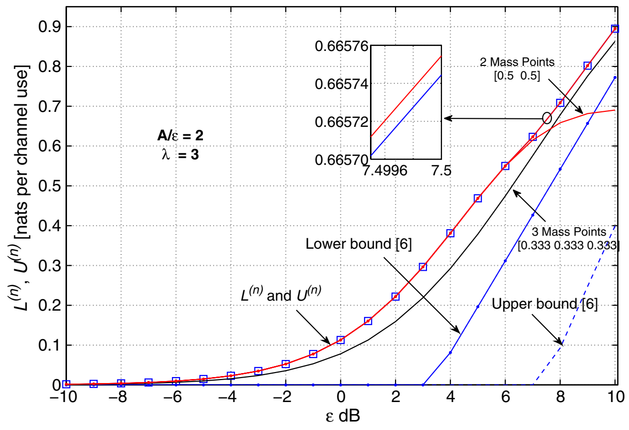

Fig. 3. (Color online) Bounds $L^{(n)}$, $U^{(n)}$ on channel capacity (on top of each other) and closed form bounds from [6] with $A/\varepsilon = 2$ and $\lambda = 3$.

demonstrates the importance of nonuniform signaling for discrete-time Poisson channels.

Figure 3 plots similar mutual information curves with peak-to-average ratio $A/\varepsilon = 2$, which is common in many optical transceivers. The analytical upper and lower bounds of Lapidoth and Moser [6, Eqs. (18) and (19)] under the same conditions are also presented. Again, the analytical bounds only yield insight for very high values of ε. Notice that equiprobable signaling achieves rates close to the capacity. Indeed, for $\varepsilon < 6.4$ dB the capacity-achieving distribution is binary and nearly uniform. Thus, nonuniform signaling is not essential in the case of $A/\varepsilon = 2$ to approach capacity. Comparing Figs. 1 and 3, however, illustrates that for a given average power consumption, large increases in channel capacity are available by increasing the peak emitted power. For spacecraft applications, ε is a metric of the lifetime of the batteries. Thus, building optical transceivers with higher peak powers and nonuniform signaling can deliver far higher rates for the same average power consumption.

C. Example: LEO Intersatellite Link

To quantify the possible gains using nonuniform signaling, consider the example of an LEO laser communication link demonstrated between TerraSAR-X and NFIRE satellites [4]. This link operates at a data rate of 5.625 Gbps over a link distance of 3800–4900 km. Table I provides a list of parameters for these terminals [4] and realistic values for the link.

A simplified link budget analysis can be used to estimate the average number of received signal photons for a link at wavelength λ_w over a range z with signaling interval T as follows [16]:

$$\varepsilon = P_T \eta_T \eta_R \frac{\eta \lambda_w}{hc} \left(\frac{\lambda_w}{4\pi z} \right)^2 G_T L_T \left(\frac{\pi d_r}{\lambda_w} \right)^2 T = 7.5027, \quad (7)$$

where P_T is the average transmitter power, η_T and η_R are efficiencies of the transmitter and receiver optics, η is the

TABLE I
TERMINAL CHARACTERISTICS

Wavelength, λ_w	1064 nm
Data rate, $1/T$	5.625 Gbps
Link distance, z	4900 km
Peak transmit power, $2P_T$	700 mW
Transmitter aperture diameter, d_t	125 mm
Transmitter optical efficiency, η_T[a]	0.5
Receiver aperture diameter, d_r	125 mm
Receiver optical efficiency, ηR[b]	0.35
Detector quantum efficiency, η[c]	0.7
Pointing error, θ_T	5 μ radian (rms)
Spectral radiance of Earth, W[d]	5×10^{-3} Watt/cm^2 – μm – sr
Receiver field-of-view, Ω[e]	2 mrad
Bandwidth of receiver filter, $\Delta\lambda$	2 nm

[a] Assume 0.5 [16].
[b] Assume 0.35 [16].
[c] Assume 0.7 [16].
[d] This value corresponds to the wavelength 1 μm [3].
[e] Typically, this value is between 1.7–2.2 mrad [4].

quantum efficiency of the detector, d_r and d_t are the aperture diameters of transmitter and receiver, h is Planck's constant, and c is the speed of light in a vacuum. The gain of the transmit antenna relative to an isotropic emitter is

$$G_T = \left(\frac{\pi d_t}{\lambda_w}\right)^2, \tag{8}$$

while the loss due to pointing error θ_T is estimated by

$$L_T = \exp(-G_T\theta_T^2). \tag{9}$$

The primary noise source of the receiver is assumed to arise from scattered light from Earth (i.e., earthshine). The average number of background photons received per signaling interval can be estimated as follows [3]:

$$\lambda = W(\lambda_w)\pi\left(\frac{dr}{2}\right)^2(\Delta\lambda)\frac{\pi}{4}\Omega^2 T\frac{\lambda_w}{hc} = 3.6649, \tag{10}$$

where $W(\lambda_w)$ is the spectral radiance of Earth, $\Delta\lambda$ is the bandwidth of the receiver filter, and Ω is the receiver field-of-view.

The capacity of the LEO intersatellite link is computed following Section III using the estimated ε and λ and shown in Fig. 4 versus the peak constraint A. As a metric of comparison, the mutual information rate achieved by the conventional uniform binary signaling scheme with the same ε and λ is computed to be $C_0 = 0.6718$ nats per channel. Figure 4 also presents the rate gain available by using nonuniform signaling over C_0.

Even for $A/\varepsilon = 2$, there is a gain in rate of 12% over the baseline uniform binary scheme C_0.[1] Thus, nonuniform signaling is useful in improving the data rate in all cases in Fig. 4. Increasing the available peak power by 50% to about 1 W gives $A/\varepsilon = 3$ and yields a 30% gain in rate over conventional binary uniform signaling for the same

[1] In fact, in this case the capacity-achieving distribution is nonuniform and ternary.

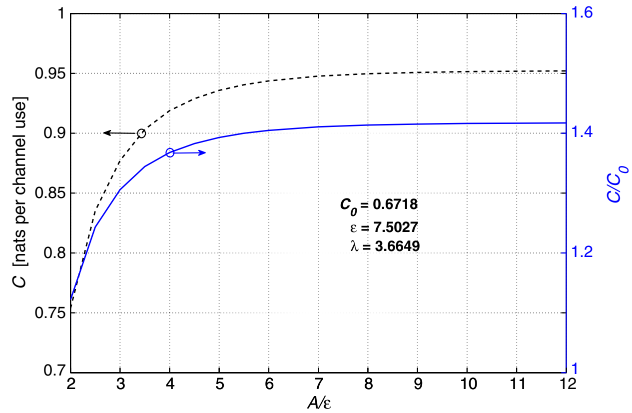

Fig. 4. (Color online) Channel capacity for LEO intersatellite link versus A/ε with $\varepsilon = 7.5027$ and $\lambda = 3.6649$. For comparison, the gain in rate versus uniform binary signaling, C_0, is also presented.

average power. Further increasing the peak constraint improves the capacity with smaller relative increases in rate. Thus, using laser emitters with larger peak powers and nonuniform signaling can yield impressive gains in the channel capacity of the LEO intersatellite link while keeping the average power consumption constant. That is, this improvement in rate does not come at the expense of increased average energy usage.

The remainder of this paper considers practical algorithms to approach these large gains in rate by employing nonuniform signaling.

IV. NONUNIFORM SIGNALING DESIGN FOR DISCRETE-TIME POISSON CHANNELS

A. Practical Constellation Design: Constrained Particle Method

The resulting capacity-achieving distribution obtained in Section III has arbitrary probability mass values that may not be practical for code design. Simply quantizing the optimal distribution does not take full advantage of the average power constraint. Consider a *constrained particle method* that incorporates the quantization levels into distribution design and is defined as follows:

1. Choose a large enough M and run the W-step and X-step of Section III iteratively until convergence to yield the capacity-achieving distribution $\{(x_i^*, p_i^*)\}$.
2. Select $N \in \mathbb{Z}^+$ according to the system requirements. In general, larger N provide more precise quantization results at the expense of complexity.
3. Enumerate all possible distributions of the form $\{(x_i^*, \hat{p}_i)\}$, where $\hat{p}_i = k/2^N$ for $k \in \{0, 1, \ldots, 2^N - 1\}$. Notice that $\sum \hat{p}_i = 1$ by definition. Denote the collection of all such distributions by $\hat{\mathcal{P}}$ and $\hat{\mathcal{P}}_\varepsilon \subseteq \hat{\mathcal{P}}$ as the collection that satisfies the average amplitude constraint.
4. If $|\hat{\mathcal{P}}_\varepsilon| > 0$ (i.e., at least one combination satisfies the average power constraint), choose the element in $\hat{\mathcal{P}}_\varepsilon$ that has the smallest Kullback–Leibler (K-L) divergence to

$\{(x_i^*, p_i^*)\}$. Then, run the X-step in Eq. (4) under the average constraint.

5. Or, no elements in $\hat{\mathcal{P}}$ satisfy the average constraint. Choose the distribution in $\hat{\mathcal{P}} - \hat{\mathcal{P}}_\varepsilon$ that has the smallest K-L divergence to $\{(x_i^*, p_i^*)\}$ and denote it $\{(\tilde{x}_i, \tilde{p}_i)\}$. Scale this distribution as $\{(\alpha\tilde{x}_i, \tilde{p}_i)\}$, where $\alpha = \varepsilon/\sum \tilde{x}_i\tilde{p}_i$ to ensure the average constraint is satisfied.

Notice that the resulting source distribution satisfies all channel constraints and has quantized probability mass values.

The mutual information of the constrained particle method with $N = 2$ and 3 as a function of $1/\lambda$ for fixed ε and A is shown in Fig. 5. For comparison, the channel capacity computed by the particle method of Section III is also presented. The largest gap between the mutual information and channel capacity is approximately 0.02 nats/channel use. Notice that as λ decreases, constellations with more quantization levels are required to approach the channel capacity.

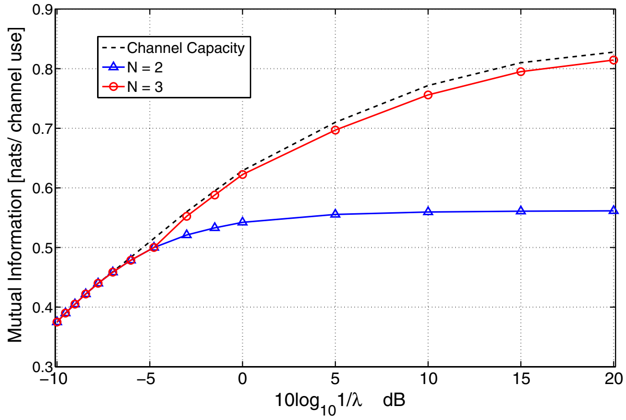

Fig. 5. (Color online) Channel capacity and mutual information for constellations from the constrained particle method for $\varepsilon = 4$ dB and $A/\varepsilon = 4$.

Figure 6 plots the capacity-achieving input distributions and the results of the constrained particle method for $\varepsilon = 4$ dB and $A/\varepsilon = 4$ with $\lambda = 10$, 4, 0.1, 0.01, respectively. When $\lambda = 10$, the capacity-achieving distribution and the constrained signal constellation coincide. For $\lambda = 4$, the output of the constrained method results in fewer mass points than the capacity-achieving distribution. Thus, the constrained technique often produces a less complex transmitter with fewer output amplitudes while remaining very close to the channel capacity.

B. Coding and Nonuniform Signaling

As seen in earlier sections, to approach the capacity of the discrete-time Poisson channel, signaling at discrete amplitudes with nonuniform probabilities is necessary. In previous work on related channels [10,11], a mapper is used to induce the correct distribution and coupled with MLC and MSD to approach capacity. In general, however, MLC-MSD suffers from error propagation and latency in decoding and requires multiple encoders and decoders.

In this work, a single code is used to encode all bits, and the mapper obtained from the constrained particle method is implemented to induce the correct distribution. At the receiver, demapping and decoding are done jointly via the sum-product algorithm.

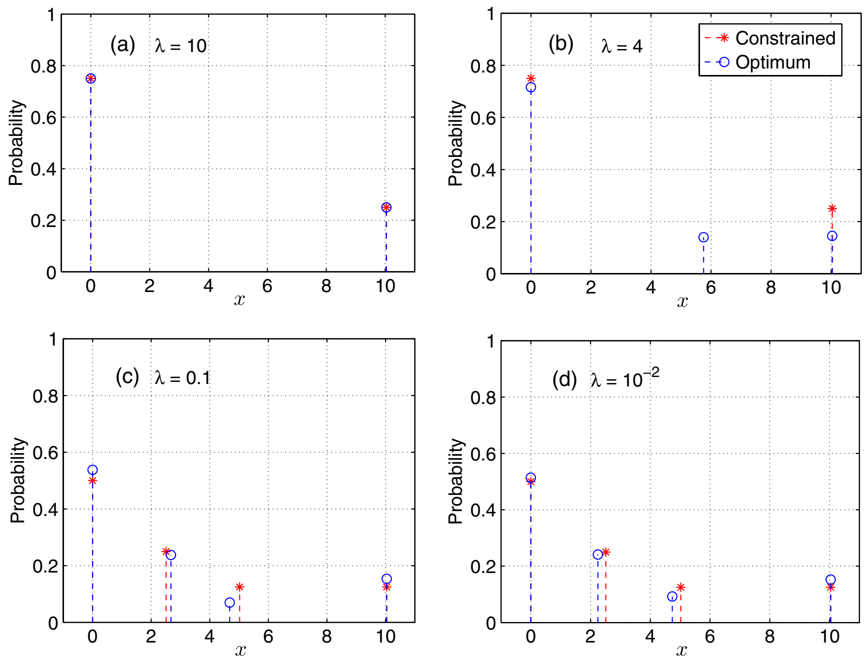

Fig. 6. (Color online) The optimum and the proposed input distribution for different λ when $\varepsilon = 4$ dB and $A/\varepsilon = 4$. For (a) and (b) $N = 2$ and for (c) and (d) $N = 3$.

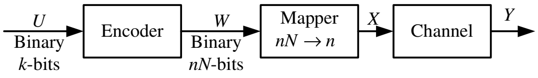

Fig. 7. System model for the developed encoding method and mapping scheme.

Figure 7 presents a block diagram of the encoder and mapper. Let the message U be composed of k bits that are assumed to be uniformly distributed and input to the LDPC encoder. Define the length of the LDPC code to be nN, where 2^N is the number of quantization steps in the constrained particle method. The value n is an integer selected so that the capacity $C > k/n$. Additionally, group the output coded bits as $(W_1^{(i)}, W_2^{(i)}, \ldots, W_N^{(i)})$, for $i = 1, 2, \ldots, n$. Notice that because the LDPC code is a linear block code, the output distribution of the symbols in W can be assumed to be uniform. Let $f\colon \{0,1\}^N \to \mathcal{X}$ be a deterministic mapper that induces the desired distribution as determined by the constrained particle method in Subsection IV.A. This mapper is straightforward to implement because all probability masses are constrained to be of the form $k/2^N$.

Thus, each block of N coded bits, indexed by i, is input to the mapper to yield a single channel input X_i.

C. Code Design: Example I

Consider channel constraints $A/\varepsilon = 4$ and $\lambda = 3$. From Fig. 2, it is apparent that for the range $-10 \le \varepsilon \le 2$ dB the capacity-achieving distribution has two mass points at $\{0, A\}$ and $p_0 = 3/4$. In this example, the encoding, mapping, and joint demapping-decoding processes are described in detail and their performance is simulated.

1) Encoding and Mapping: For $N = 2$ and assuming uniformly distributed input bits, the mapper f induces the desired distribution

$$(W_1^{(i)} W_2^{(i)}) \overset{f}{\mapsto} X{:}X = \begin{cases} A, & W_1^{(i)} = W_2^{(i)} = 1, \\ 0, & \text{otherwise}. \end{cases} \tag{11}$$

The equivalent channel seen by bit W_1 (and W_2 due to the symmetry of the mapper) can be found by marginalizing the conditional probability

$$\begin{aligned} P_{Y|W}(y|w_1 = 1) &= \sum_{w_2} P_{Y|X}(y, w_2|w_1 = 1) \\ &= \frac{1}{2} P_{Y|X}(y|A) + \frac{1}{2} P_{Y|X}(y|0), \\ P_{Y|W}(y|w_1 = 0) &= P_{Y|X}(y|0), \end{aligned}$$

where $P_{Y|X}(\cdot|\cdot)$ is the channel law.

2) Joint Demapping and Decoding: Consider representing the LDPC code and the mapper together in a factor graph. An example for $N = 2$ with the mapper in Eq. (11) is presented in Fig. 8. Message passing on this graph using the sum-product algorithm can demap and decode the bits jointly.

The lower part of the graph represents a traditional LDPC code and the mapping function f is represented by the triangular nodes. Furthermore, both $w^{(i)}$ and x_i are binary in this example. Following the standard sum-product algorithm [17], the message from the mapper to the message bit $w_1^{(i)}$ is

$$\begin{aligned} \mu_{f\to w_1^{(i)}}(w_1^{(i)} = 1) &= \mu_{x_i\to f}(x_i = A)\mu_{w_2^{(i)}\to f}(w_2^{(i)} = 1) \\ &\quad + \mu_{x_i\to f}(x_i = 0)\mu_{w_2^{(i)}\to f}(w_2^{(i)} = 0), \\ \mu_{f\to w_1^{(i)}}(w_1^{(i)} = 0) &= \mu_{x_i\to f}(x_i = 0)\mu_{w_2^{(i)}\to f}(w_2^{(i)} = 1) \\ &\quad + \mu_{x_i\to f}(x_i = 0)\mu_{w_2^{(i)}\to f}(w_2^{(i)} = 0). \end{aligned}$$

An analogous message from f to $w_2^{(i)}$ is also simple to derive based on Eq. (11).

For this example, the message from x_i to f can be written as the log-likelihood ratio

$$\begin{aligned} m_{x_i\to f} &= \ln \frac{\mu_{x_i\to f}(x_i = 0)}{\mu_{x_i\to f}(x_i = 1)} = \ln \frac{P(x_i = 0|y_i)}{P(x_i = 1|y_i)} \\ &= \ln \frac{3P(y_i|x_i = 0)}{P(y_i|x_i = A)}. \end{aligned} \tag{12}$$

All other message passing for the LDPC code takes place in the standard manner [18]. Due to the symmetry of the mapper in $w_1^{(i)}$ and $w_2^{(i)}$, the update rules for both are the same. After several rounds of message passing, a hard decision is made for each $w^{(i)}$.

3) Simulation on BER Performance: Notice that the previous discussion of the joint demapping-decoding technique depends only on the particular mapper chosen. To have a concrete example, referring to Fig. 1, the channel capacity when $\varepsilon = -1.21$ dB, $A/\varepsilon = 4$, and $\lambda = 3$ is approximately 0.2438 bits (0.169 nats) per channel use. As shown in Fig. 2, the capacity-achieving distribution in this case has two amplitude points at 0 and A and has probability mass $p_0 = 0.75$ corresponding to the previously developed mapper (for $N = 2$).

To realize the code design for this system, an LDPC code with rate $R = 0.12$ bits/channel use is required since two encoded symbols are mapped to a channel symbol. An LDPC code with rate 0.12 bits/channel use is designed using [19] for an additive white Gaussian noise (AWGN) channel to yield the degree distributions

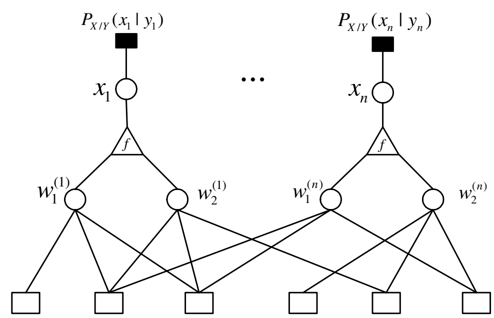

Fig. 8. Developed factor graph for joint demapping and decoding.

$$\lambda(x) = 0.5513x + 0.2031x^2 + 0.0917x^4 + 0.0045x^6 + 0.017x^7 + 0.0995x^8 + 0.033x^9,$$
$$\rho(x) = x^2.$$

The total length of the code is set to 10,000 bits, which corresponds to 5000 transmitted channel symbols.

The BER performance of the system is shown in Fig. 9 versus $1/\lambda$ for ε and A fixed. The figure indicates the point corresponding to $\lambda = 3$, which was used for design. Notice that the BER drops as $1/\lambda$ increases. For comparison, a uniform distribution that satisfies the same average power constraint is also considered. At $1/\lambda = 1.31$, the information rate using uniform signaling is 0.24 bits/channel use, which is identical to the designed rate. Clearly, uniform signaling is quite far from the channel capacity, and a nonuniform signaling scheme, such as the one presented here, is required to take full advantage of discrete-time Poisson channels.

D. Code Design: Example II

Consider the design of a nonuniform mapper and coding scheme under the conditions for an LEO intersatellite link described in Subection III.C (i.e., $\varepsilon = 7.5027$ and $\lambda = 3.6649$). A value of $A/\varepsilon = 2.62$ is selected (from Fig. 4) because the channel capacity is approximately 25% greater than the uniform signaling case (i.e., 1.22 bits/channel use). Notice that this is a mild increase in the peak-to-average ratio over the uniform system, which inherently has $A/\varepsilon = 2$. The goal of this example is to quantify the practical gains in rate that can be realized by exploiting the small increase in peak amplitude for the same ε and λ.

1) Encoding and Mapping: For $\varepsilon = 7.5027$, $\lambda = 3.6649$, and $A/\varepsilon = 2.62$, the channel capacity is 1.22 bits/channel use, which is achieved by the following input distribution:

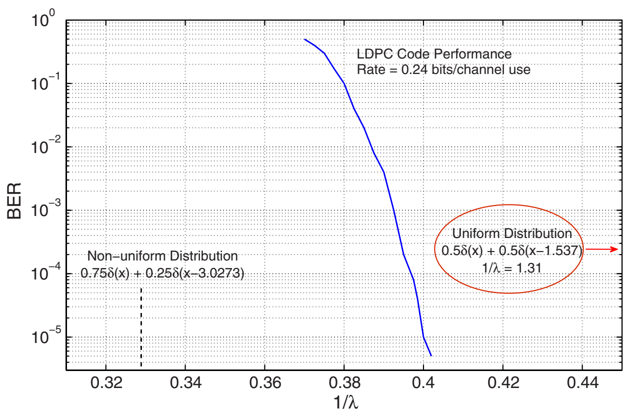

Fig. 9. (Color online) BER versus $1/\lambda$ for the nonuniform signaling using finite-length LDPC codes for $\varepsilon = -1.21$ dB, $A/\varepsilon = 4$. The value of $1/\lambda$ corresponding to optimal uniform (out of range) and nonuniform signaling at 0.24 bits/channel use is presented for comparison.

$$p_X^*(x) = 0.4444\delta(x) + 0.2001\delta(x-7.1835) + 0.0883\delta(x-9.2315) + 0.2672\delta(x-19.6503).$$

Setting $N = 2$ in the constrained particle method results in the following distribution:

$$\hat{p}_X^*(x) = 0.5\delta(x) + 0.25\delta(x-8.76) + 0.25\delta(x-19.6505), \quad (13)$$

with the mutual information rate 1.20 bits/channel use.

Notice that this distribution can be induced through the simple mapper f

$$(W_1^{(i)}W_2^{(i)}) \overset{f}{\mapsto} X : X = \begin{cases} A_0, & W_1^{(i)} = 0 \\ A_1, & W_1^{(i)} = 1, \quad W_2^{(i)} = 0, \\ A_2, & W_1^{(i)} = 1, \quad W_2^{(i)} = 1 \end{cases} \quad (14)$$

where $A_0 = 0$, $A_1 = 8.76$, and $A_2 = 19.6505$.

The equivalent channel seen by bit W_1 and W_2 as well as the message passing rules can be found by simple extension of the results in Subsection IV.C.

2) Simulation on BER Performance: Since the information rate with the input in Eq. (13) when $\lambda = 3.6649$ is 1.20 bits/channel use, an LDPC code with rate $R =$ 0.568 bits/channel use and degree distributions [20]

$$\lambda(x) = 0.181804x + 0.197579x^2 + 0.011671x^3 + 0.098834x^4 + 0.063856x^5 + 0.239152x^{24} + 0.207105x^{25},$$
$$\rho(x) = 0.839350x^{10} + 0.160650x^{11}$$

is applied in the this system with a code length of 10,000 bits.

Figure 10 plots the BER of the coding system with mapper in Eq. (14) versus $1/\lambda$. The BER of the joint coding-mapping system is less than 10^{-5} for the target $\lambda = 3.6649$ computed in the LEO link budget (Subsection III.C). Thus, for the same ε and λ, the resulting system has a rate that is

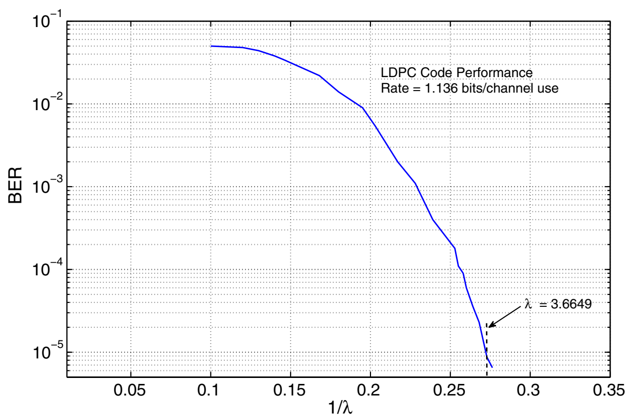

Fig. 10. (Color online) BER versus $1/\lambda$ for the nonuniform signaling using finite-length LDPC codes with $R = 1.136$ bits/channel use as $\varepsilon = 7.5027$, $A/\varepsilon = 2.62$.

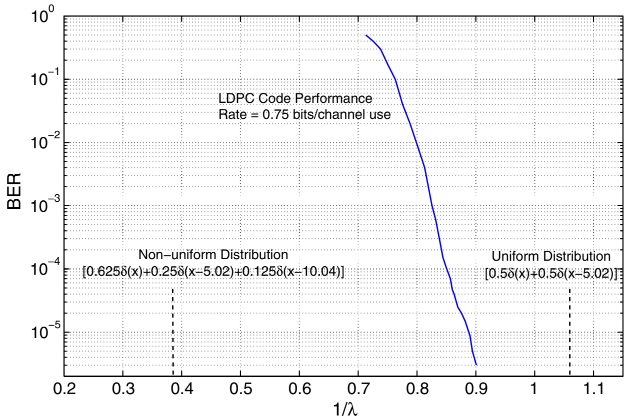

Fig. 11. (Color online) BER versus $1/\lambda$ for the nonuniform signaling using finite-length LDPC codes as $\varepsilon = 4$ dB, $A/\varepsilon = 4$. The $1/\lambda$ corresponding to optimal uniform signaling and nonuniform signaling with $R = 0.75$ bits/channel use is presented for comparison.

17% larger than that of uniform signaling (i.e., C_0). This corresponds to a data rate of 6.6 Gbps. This increase in rate, however, is achieved at the expense of an increase in peak-to-average ratio from 2 to 2.62.

E. Code Design: Example III

In some cases to approach the channel capacity an $N = 3$ encoder and decoder are necessary. For example, from Fig. 5, for $\varepsilon = 2.51$, $A/\varepsilon = 4$, and $\lambda = 2.59$, the channel capacity is 0.7668 bits per channel use. Applying the $N = 3$ constrained particle method yields the following distribution:

$$p(0) = \frac{5}{8}, \qquad p\left(\frac{A}{2}\right) = \frac{2}{8}, \qquad p(A) = \frac{1}{8}, \tag{15}$$

and the corresponding mutual information is 0.75 bits/channel use.

Symbols are drawn three at a time from an LDPC code with rate $R = 0.25$ bits/channel use and applied to the mapping function f, defined in Eq. (16), to yield a channel symbol. An LDPC code of length 12,000 bits with rate $R =$ 0.25 bits per channel use and the degree distributions [20]

$$\lambda(x) = 0.602x + 0.238x^2 + 0.0309x^3 + 0.021x^4 + 0.0491x^5 + 0.0141x^6 + 0.0208x^7 + 0.023x^8 + 0.001x^9,$$

$$\rho(x) = 0.0001x + 0.1017x^2 + 0.8982x^3$$

is combined with the mapper f in Eq. (16):

$$W = [W_1 W_2 W_3] \overset{f}{\mapsto} X{:}X = \begin{cases} A_0, & W_1 = 0, \\ A_0, & W_1 = 1, W_2 = 1, W_3 = 0, \\ A_1, & W_1 = 1, W_2 = 0, W_3 = 0, \\ A_1, & W_1 = 1, W_2 = 0, W_3 = 1, \\ A_2 & W_1 = W_2 = W_3 = 1. \end{cases} \tag{16}$$

The equivalent channel law as well as the messages passed during the sum-product algorithm can be derived in a similar fashion to those in the example in Subsection IV.C.

The BER performance of the system is shown in Fig. 11 versus $1/\lambda$ for ε and A fixed. For the nonuniform distribution in Eq. (15), at $1/\lambda = 0.389$, the information rate is identical to the design rate; however, to implement the rate 0.75 bits/channel use with the BER less than 10^{-5}, $1/\lambda = 0.89$ is needed for this system. The information rate with the input in Eq. (15) and $1/\lambda = 0.89$ is about 0.886 bits/channel use. A uniform distribution with the same average power constraint has an information rate equal to 0.75 bits/channel use when $1/\lambda = 1.068$. Therefore, the practical coding scheme illustrated here is reliable at a higher value of λ than the optimal uniform signaling scheme satisfying the same average optical power constraint.

V. Conclusion

This work presents capacity calculations and a nonuniform signaling design for intersatellite discrete-time Poisson channels corrupted by dark current under peak and average power constraints. On the basis of a realistic link budget of an LEO satellite communication link, for a given average power, significant gains in rate can be achieved using nonuniform signaling with a modest increase in peak power. Thus, nonuniform signaling is necessary and important to extract the maximum rate from such intersatellite communication links.

The channel capacity and the capacity-achieving distribution are found by adapting a particle-based Blahut–Arimoto algorithm. A constrained particle method is also developed that leads to practical signal constellations that can be applied directly to code design. A joint demapper–decoder using the sum-product algorithm is developed and requires a single encoder and decoder. Three code design examples, including the one based on the practical parameters of the LEO satellite link, are presented to quantify performance.

Simulation results show that the rate performance is close to the capacity with the BER less than 10^{-5} and far outperforms uniform signaling schemes in all scenarios. For the LEO example, for typical values of ε and λ, a gain in rate of 17% over uniform signaling is realized with practical codes at a cost of moderate peak amplitude increase.

Future work includes optimizing the degree distribution of the parity check matrix for this channel through density evolution to achieve better performance and extending results to downlink LEO-to-ground scenarios.

References

[1] R. J. McEliece, E. R. Rodemich, and A. L. Rubin, “The practical limits of photon communication,” Deep Space Network Progress Report 42–55, Jet Propulsion Laboratory, Pasadena, CA, 1979, pp. 63–67.

[2] R. J. McEliece, "Practical codes for photon communication," *IEEE Trans. Inf. Theory*, vol. IT-27, no. 4, pp. 393–398, July 1981.

[3] R. M. Gagliardi and S. Karp, *Optical Communications*. New York, NY: John Wiley & Sons, 1995.

[4] R. Fields, C. Lunde, R. Wong, J. Wicker, J. Jordan, B. Hansen, G. Muehlnikel, W. Scheel, U. Sterr, R. Kahle, and R. Meyer, "NFIRE-to-TerraSAR-X laser communication results: satellite pointing, disturbances, and other attributes consistent with successful performance," *Proc. SPIE*, vol. 7330, 73300Q, 2009.

[5] S. Shamai, "Capacity of a pulse amplitude modulated direct detection photon channel," *Proc. Inst. Elec. Eng.*, vol. 137, no. 6, pp. 424–430, Dec. 1990.

[6] A. Lapidoth and S. M. Moser, "On the capacity of the discrete-time Poisson channel," *IEEE Trans. Inf. Theory*, vol. 55, no. 1, pp. 303–322, Jan. 2009.

[7] A. Lapidoth, J. H. Shapiro, V. Venkatesan, and L. Wang, "The discrete-time Poisson channel at low input powers," *IEEE Trans. Inf. Theory*, vol. 57, no. 6, pp. 3260–3272, June 2011.

[8] A. Martinez, "Spectral efficiency of optical direct detection," *J. Opt. Soc. Am. B*, vol. 24, no. 4, pp. 739–749, Apr. 2007.

[9] R. Gallager, *Information Theory and Reliable Communication*. New York, NY: John Wiley & Sons, 1968.

[10] J. Jiang and K. R. Narayanan, "Multilevel coding for channels with non-uniform inputs and rateless transmission over the BSC," in *Proc. IEEE Int. Symp. Information Theory*, Seattle, WA, 2006, pp. 518–522.

[11] A. A. Farid and S. Hranilovic, "Channel capacity and non-uniform signalling for free-space optical intensity channels," *IEEE J. Sel. Areas Commun.*, vol. 27, no. 9, 1553–1563, Dec. 2009.

[12] J. Dauwels, "Computation of the capacity of continuous memoryless channels and the rate distortion function of memoryless continuous sources," Institute of Electronics, Information and Communication Engineers, Japan, Tech. Rep. IT2006 7-12, 2006.

[13] H. Hemmati, *Deep Space Optical Communications*. New York, NY: John Wiley & Sons, 2006.

[14] S. B. Alexander, *Optical Communications Receiver Design*. Bellingham, WA: SPIE Optical Engineering Press, 1997.

[15] R. Blahut, "Computation of channel capacity and rate-distortion functions," *IEEE Trans. Inf. Theory*, vol. 18, pp. 460–473, 1972.

[16] C. C. Chen and C. S. Gardner, "Impact of random pointing and tracking errors on the design of coherent and incoherent optical intersatellite communication links," *IEEE Trans. Commun.*, vol. 37, pp. 252–260, Mar. 1989.

[17] F. R. Kschischang, B. J. Frey, and H.-A. Loeliger, "Factor graphs and the sum-product algorithm," *IEEE Trans. Inf. Theory*, vol. 47, no. 2, pp. 498–519, Feb. 2001.

[18] T. Richardson, A. Shokrollahi, and R. Urbanke, "Design of capacity-approaching irregular low-density parity-check codes," *IEEE Trans. Inf. Theory*, vol. 47, pp. 619–637, Feb. 2001.

[19] EPFL Information Processing Group, "LDPC degree distribution optimizer for Gaussian channel" [Online]. Available: http://lthcwww.epfl.ch/research/ldpcopt.

[20] Signal Processing Microelectronics, University of Newcastle, "LOPT—online optimisation of LDPC and RA degree distributions" [Online]. Available: http://sonic.newcastle.edu.au/ldpc/lopt/index.php.

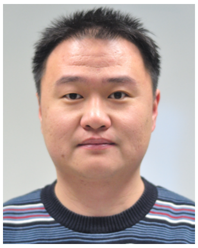

Jihai Cao received the B.A.Sc. and M.A.Sc degrees with honors in electrical engineering from Harbin Institute of Technology, China, in 2006 and 2008, respectively. He currently is pursuing the Ph.D. degree in electrical and computer engineering at McMaster University, Canada. His field of interest includes wireless optical communication, information theory, and coding.

Steve Hranilovic (S'94–M'03–SM'07) received the B.A.Sc. degree with honors in electrical engineering from the University of Waterloo, Canada, in 1997 and M.A.Sc. and Ph.D. degrees in electrical engineering from the University of Toronto, Canada, in 1999 and 2003, respectively.

He currently is an associate professor in the Department of Electrical and Computer Engineering, McMaster University, Hamilton, Ontario, Canada. During 2010–2011, he spent his research leave as a senior member, technical staff in advanced technology, for Research in Motion, Waterloo, Canada. His research interests are in the areas of free-space and wired optical communications, digital communication algorithms, and electronic and photonic implementation of coding and communication algorithms. He is the author of the book *Wireless Optical Communications Systems* (New York: Springer, 2004).

He is a licensed professional engineer in the Province of Ontario and was awarded the government of Ontario Early Researcher Award in 2006. He currently serves as an associate editor for the *IEEE Transactions on Communications* in the area of optical wireless communications.

Jun Chen (S'03–M'06) received the B.E. degree with honors in communication engineering from Shanghai Jiao Tong University, Shanghai, China, in 2001, and the M.S. and Ph.D. degrees in electrical and computer engineering from Cornell University, Ithaca, NY, in 2004 and 2006, respectively.

He was a postdoctoral research associate in the Coordinated Science Laboratory at the University of Illinois at Urbana-Champaign, Urbana, IL, from 2005 to 2006, and a postdoctoral fellow at the IBM Thomas J. Watson Research Center, Yorktown Heights, NY, from 2006 to 2007. He currently is an assistant professor of electrical and computer engineering at McMaster University, Hamilton, ON, Canada. He holds the Barber-Gennum Chair in Information Technology. His research interests include information theory, wireless communications, and signal processing.

He has received several awards for his research, including the Josef Raviv Memorial Postdoctoral Fellowship in 2006, the Early Researcher Award from the Province of Ontario in 2010, and the IBM Faculty Award in 2010.